JOURNAL OF CATALYSIS 54, 414–425 (1978)

The Characterization of Surface Carbides of Tungsten

J. B. BENZIGER, E. I. KO, AND ROBERT J. MADIX

Department of Chemical Engineering, Stanford University, Stanford, California 94305

Received December 27, 1977; revised July 3, 1978

The properties of surface carbides of tungsten single crystals were studied using LEED, AES, and thermal desorption spectroscopy. Carburization of W(100) produced a series of surface structures; at $\theta = 0.5$ a $c(2 \times 2)$ structure was observed which compressed into a double row $\begin{pmatrix} 3 & 0 \\ 1 & -1 \end{pmatrix}$ structure at $\theta = 0.67$. This surface was inert to further carburization below 1000 K. Heating the crystal to 1500 K in ethylene resulted in the formation of an interstitial carbon layer having the structure of ditungsten carbide at the surface. The dissociative adsorption of hydrogen and CO were inhibited by adsorbed carbon or oxygen occupying fourfold symmetry interstitial sites on the W(100) surface. Dissociative adsorption of CO was directly related to the number of pairs of unoccupied fourfold sites. Adsorption of molecular CO correlated with the number of surface sites passivated by adsorbed carbon or oxygen. A surface passivated by dissociatively adsorbed CO was found to behave qualitatively similarly to a carbide surface.

1. INTRODUCTION

The modification of metals by alloying offers the opportunity for the creation of new catalytic materials. Recent studies (*1*, *2*) have shown that alloying with carbon confers to very active metals some of the catalytic properties characteristic of more noble metals. The use of single crystals allows one to examine carefully the effect of carbon on the catalytic properties of a metal. It has been shown, for example, that the formation of a carbon chemilayer on Ni(110) results in a material that behaves more like copper (*1*).

The catalytic properties of tungsten–carbon alloys have aroused a great deal of interest. Boudart and Levy (*2*) found that tungsten carbide (WC) displayed "platinum-like" behavior for several test reactions. Tungsten carbide was also found to compare favorably with platinum as an electrode for the oxidation of hydrogen (*3*). Ross and Stonehart (*4–6*) examined the effect of surface composition on the electrocatalytic activity of WC and found the greatest activity was recorded for samples that were slightly carbon deficient. Recently, Boudart and Imura (*7*) found that the platinum-like behavior of WC is dependent upon the chemical state of the surface carbon, graphitic carbon producing very inactive surfaces. This paper reports the effects of surface carbon on the chemisorption properties of tungsten for CO and H_2 obtained using the combined techniques of Auger electron spectroscopy (AES), low-energy electron diffraction (LEED), and flash desorption spectroscopy (FDS).

The carburization of W(100), W(110), and W(111) was studied by Boudart and Ollis (*8*) using LEED and X-ray diffraction. They found a series of stable

0021-9517/78/0543-0414$02.00/0

surface structures which culminated in the formation of a ditungsten carbide overlayer in registry with the tungsten substrate. Similar results were reported by others (*9–12*) for both W(110) and W(211). In this work studies of the carburization of W(100) and W(110) using LEED and AES are reported in which the results from both techniques were correlated to deduce the stable intermediate structure on W(100).

As a probe of the chemical activity of the surfaces, the chemisorption of H_2 and CO was examined with FDS. The results indicated that a surface carbide confers behavior more characteristic of noble metals than of tungsten. In particular, the ability of tungsten to dissociate CO and H_2 was found to be quite sensitive to the presence of surface carbon.

2. EXPERIMENTAL

The experiments were carried out in a stainless-steel UHV chamber pumped by a 220 liter/sec Noble Vac-Ion pump and a titanium sublimation pump. After a bakeout, base pressures of less than 2×10^{-10} Torr (2.7×10^{-8} Pa) were achieved. The system contained PHI four-grid LEED optics, a UTI quadrupole mass spectrometer, an argon ion bombardment gun, and a PHI cylindrical mirror analyzer (CMA). A schematic diagram of the apparatus is shown in Fig. 1.

The oriented tungsten crystals were in the form of thin disks (10×0.5 mm). They were cut from high-purity single crystals to the desired orientation and then ground with diamond paste. The disk was supported on a tungsten clip clamped to a sapphire rod for electrical insulation. The sample could be heated linearly with time up to 1000 K by radiation from a tungsten filament located 3 mm behind the sample. A heating rate of 20 K/sec was used in all experiments other than heating rate variation studies. Temperatures above 1000 K were achieved with electron bombardment; the sample was floated at +1500 V; the emission current from the tungsten filament to the sample was then varied to achieve the desired temperature. Cooling of the sample was achieved by heat conduction through the sapphire rod which was in thermal contact with a liquid nitrogen reservoir.

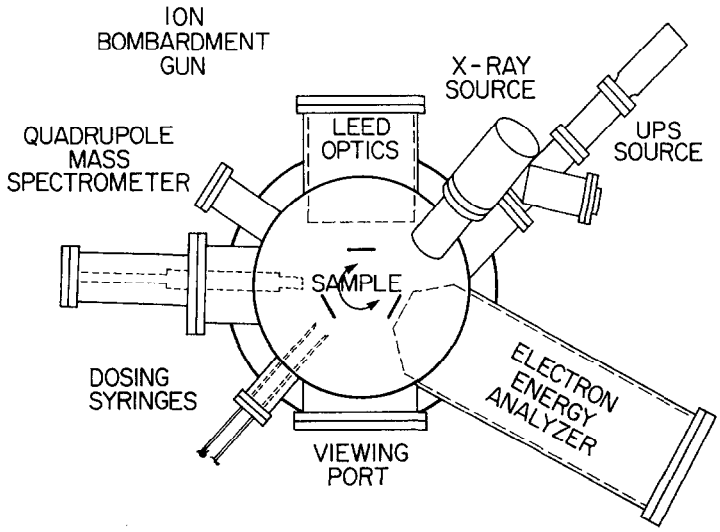

FIG. 1. Schematic of the apparatus.

This arrangement allowed cooling of the sample from 2500 K to 250 K within 5 min, and to 100 K within 30 min. Tungsten–5% rhenium, tungsten–26% rhenium thermocouple leads were spot-welded onto the back of the crystal to monitor the temperature.

Surface composition was monitored by AES. The Auger spectra were obtained using a double-pass cylindrical mirror analyzer fitted with an integral electron gun at normal incidence operated at 3 keV. Beam currents were typically 20 μA, permitting rapid scanning of the energy range, 0 to 600 eV. Scanning different regions of the surface indicated that electron beam effects were negligible.

The tungsten crystal was cleaned by heating to 1500 K in 5×10^{-6} Torr (6.7×10^{-4} Pa) of oxygen for 2 to 3 hr and then flashing to 2500 K under vacuum. This produced a clean surface as characterized by AES and LEED. There were always trace amounts of carbon and oxygen which could not be removed by this cleaning procedure; however, these represented less than 2% of a monolayer. Determination of the amount of surface carbon and oxygen was based on the ratio of the peak heights of the W(350) to the C(271), and the O(510) transitions as calibrated by coverage of the CO(β) state. These particular transitions were chosen as the peak shapes did not change, and they were easily isolated.

Gases were admitted for adsorption through a variable leak valve connected to a 22-gauge stainless-steel syringe (0.34 mm i.d.) which produced a highly directed beam to the front side of the crystal. The distance between the end of the syringe and the sample was approximately 1 cm, which assured a uniform flux across the surface. For most of the flash desorption experiments the crystal was rotated to directly face the ionizer of the mass spectrometer enhancing the signal-to-noise ratio during desorption. Absolute coverages were determined by rotating the sample so there was no line of sight from the crystal face to the ionizer of the mass spectrometer, permitting measurements of partial pressure vs temperature. The pumping speed was measured from the decay of a pressure burst from a tungsten filament. Pumping speed measurements were reproducible to within 10%. The surface coverage was then determined from the area under the flash desorption curve,

$$N = \frac{SK}{A\beta G} A_{FD},$$

where N = coverage (molecules/cm^2); S = pumping speed (liter/sec); $K = 3.3 \times 10^{19}$ molecules/Torr/liter; β = heating rate (°K/sec); G = gain of mass spectrometer (A/Torr); A = area of crystal face (cm^2); and A_{FD} = area under flash desorption curve (A-K). The surface coverages reported were reproducible to within 15%.

The gases used in these studies were: (1) ethylene, Matheson 99.5%, (2) oxygen, Matheson 99.6%, (3) hydrogen, Matheson 99.5%, and (4) carbon monoxide, Matheson 99.5%. Mass scans of the gases always showed greater than 95% purity upon admission of the gas to the UHV system.

3. RESULTS

3.1. LEED and AES Study of the Carburization of Tungsten

In order to determine the amount of surface carbon from AES it was necessary to find a calibration standard. As standards two coverages of CO(β) on W(100) were chosen. The β state of CO on W(100) has been shown to be dissociatively adsorbed (*13*). Figure 2a is an Auger spectrum of W(100) saturated with CO and then heated to 500 K to desorb the molecularly bound CO(α). The carbon Auger signal showed the three peak structure characteristic of tungsten carbide exem-

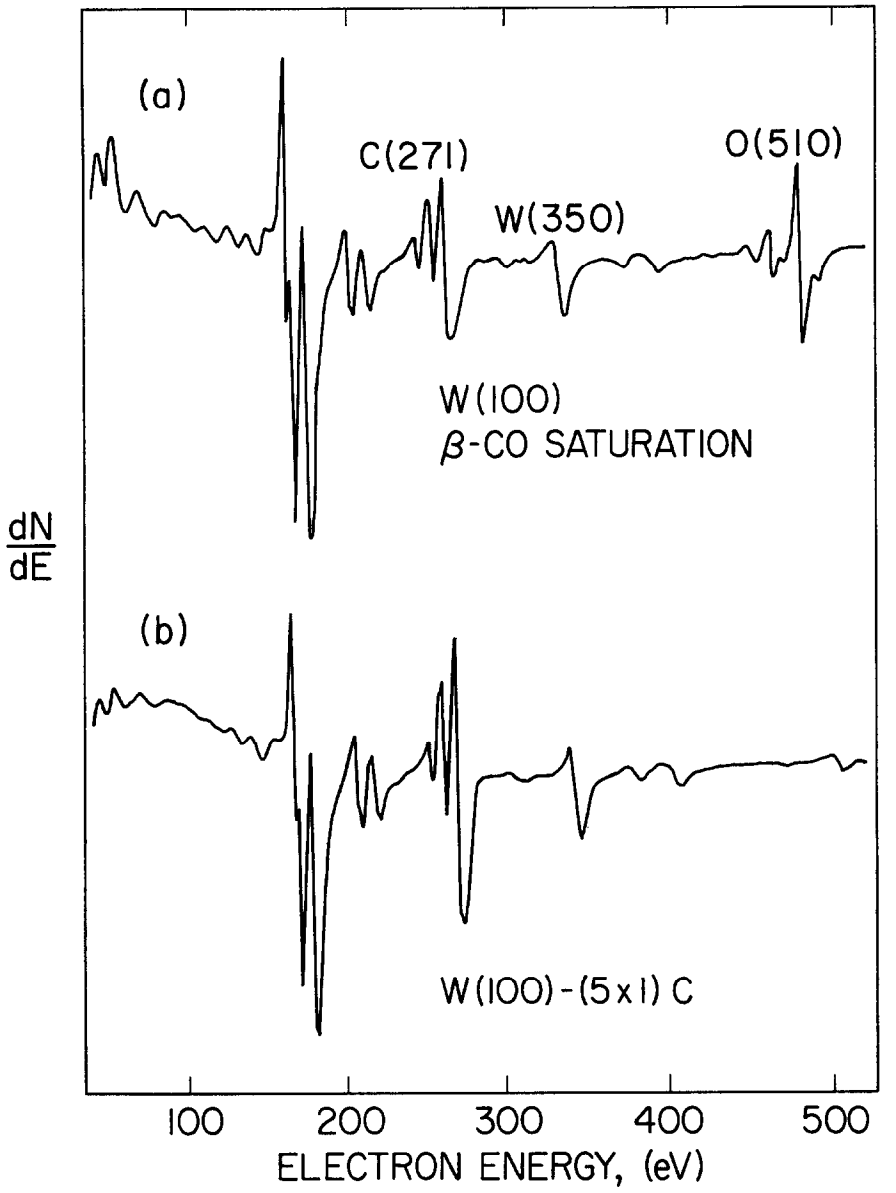

FIG. 2. (a) Auger spectrum of W(100) surface saturated by CO(β); (b) Auger spectrum of W(100)-(5 × 1)C.

plified in Fig. 2b, allowing this to be used as a calibration. The CO(β) saturation coverage has been measured by others (*14*, *15*) to be $4.3 \pm 0.2 \times 10^{14}$ molecules/cm^2. Comparison of the peak heights for the C(271) Auger transition to the W(350) transition gave a relative sensitivity of C(271) to W(350) of 5.1 ± 0.2. A second coverage of CO(β) corresponding to a coverage of 2.5×10^{14} molecules/cm^2 was also used for calibration. This coverage corresponded to a $c(2 \times 2)$ LEED pattern obtained by heating the CO(β)-saturated surface to 1100 K. Based on this coverage the relative Auger yield of C(271) to W(350) was 5.2 ± 0.3.

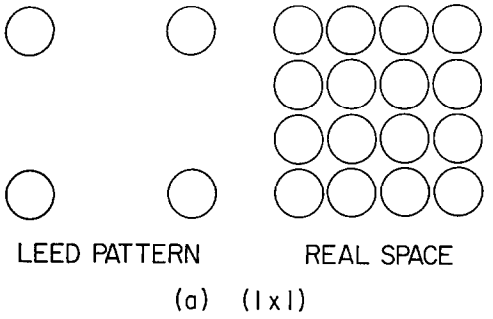

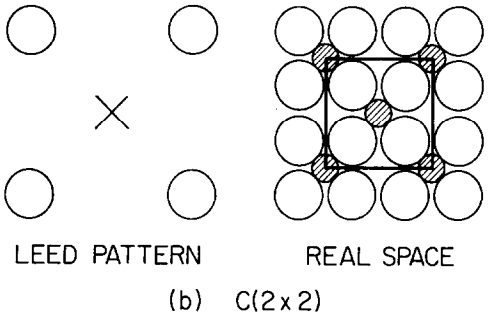

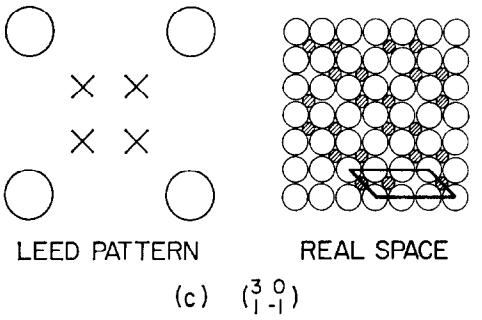

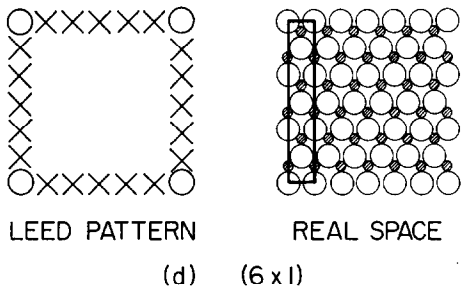

FIG. 3. LEED patterns and real space interpretations: (a) W(100) clean; (b) W(100)-$c(2 \times 2)$C; (c) W(100)-$\begin{pmatrix} 3 & 0 \\ 1 & -1 \end{pmatrix}$C; (d) W(100)-$(6 \times 1)$C; (e) W(100)-$(5 \times 1)$C; (f) W(100)-$(15 \times 5)$R14°C. ▨, carbon; ○, tungsten; ●, tungsten second layer.

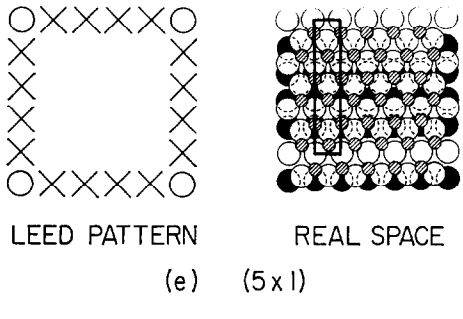

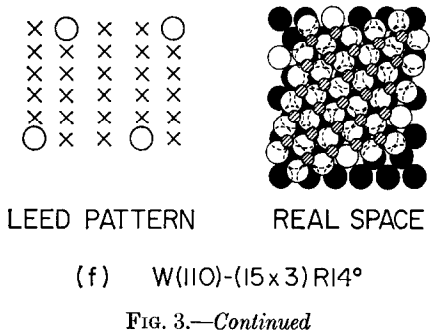

FIG. 3.—*Continued*

In order to deduce the intermediate structures of the LEED patterns on W(100) the LEED patterns were correlated with the carbon coverages deduced from the Auger spectra utilizing the relative Auger yields of C(271) to W(350) of 5.1 for carbon adatoms. In all our studies it was found that the W(350) Auger peak height was constant for adlayer coverages of one monolayer or less, so the measured ratio of C(271) to W(350) was directly proportional to the amount of surface carbon.

Initial carburization was done by exposing the tungsten to ethylene at room temperature, followed by heating the sample to 1000 K. On W(100) this led to the gradual emergence of $c(2 \times 2)$ diffraction spots. The Auger signal ratio of C(271) to W(350) at maximum intensity of the $c(2 \times 2)$ diffraction spots was 2.6 ± 0.1, corresponding to half monolayer coverage of 5.0×10^{14} atoms/cm^2 (see Fig. 3b). Further exposure to ethylene at room temperature caused the $c(2 \times 2)$

TABLE 1

Correlation of LEED and AES

LEED pattern	Carbon atom density	AES signal ratio, C(271)/W(350)
W(100)	0	0
W(100)–CO(β) sat.	4.3×10^{14}	2.2 ± 0.1
W(100)–$c(2 \times 2)$CO(β)	2.5×10^{14}	1.3 ± 0.1
W(100)–$c(2 \times 2)$C	5.0×10^{14}	2.5 ± 0.1
W(100)–$\begin{pmatrix} 3 & 0 \\ 1 & -1 \end{pmatrix}$C	6.7×10^{14}	3.2 ± 0.1
W(100)–(6×1)C	1.0×10^{15}	3.3 ± 0.1
W(100)–(5×1)C	1.2×10^{15}	3.9 ± 0.1
W(110)–(15×3)R14°C	1.2×10^{15}	3.9 ± 0.2

diffraction spots to split into four lobes moving outward along the diagonals of the (1×1) pattern until the resultant $\begin{pmatrix} 3 & 0 \\ 1 & -1 \end{pmatrix}$ pattern was observed.[1] The C(271)/W(350) Auger yield was 3.2 ± 0.1 corresponding to $\frac{2}{3}$ monolayer coverage, suggestive of the surface structure shown in Fig. 3c. Subsequent exposure of this surface to ethylene at temperatures below 800 K caused no change in either the LEED pattern or the Auger spectrum.

When the W(100) sample was heated to 1500 K in the presence of ethylene, surface reconstruction took place, yielding new LEED patterns. A (6×1) LEED pattern was observed with the Auger signal ratio of 3.3 ± 0.2. The culmination of the carburization was a (5×1) LEED pattern with an Auger signal ratio of 3.9 ± 0.1. Further exposure to ethylene at temperatures below 2000 K resulted in no changes. Previous investigators (*8, 9*) have interpreted the (5×1) LEED pattern as a (0001) ditungsten carbide overlayer coincident on the tungsten (100) substrate, as shown in Fig. 3e. This structure has a carbon atom density of 1.2×10^{15} atoms/cm^2 which should yield a C(271)/W(350) AES signal ratio of 6.0 if the carbon atoms resided on the surface. The large discrepancy between this value and the experimentally determined value was resolved if the surface was assumed to reconstruct so that the carbon atoms were positioned in interstitial positions between the top two layers of tungsten atoms in similar fashion to the layered structure of W_2C (*17*). If the vertical distance of carbon below the surface tungsten atoms was taken to be 2.4 Å, as in W_2C, and the electron escape depth was taken from the "universal curve" to be 6 Å for the 270-V Auger electrons (*18*), the attenuated Auger intensity was calculated to be 4.0, in agreement with the observed value. The W(100)–(5×1)C surface appeared quite stable, showing only slight degradation after several days of experimentation. Continued cleaning and carburization of the surface resulted in faceting of the W(100) surface, as evidenced by splitting of the (1×1) LEED spots on certain areas of the crystal. These facets did not effect the LEED–Auger results nor the flash desorption experiments.

Similar results were obtained for W(110) carburized at 1500 K in ethylene. The only LEED pattern observed was a (15×3)R14° pattern, with an Auger signal ratio of C(271)/W(350) equal to 3.9 ± 0.2. The (15×3)R14° pattern was previously interpreted as a (0001) face of ditungsten carbide coincident on the (110) tungsten substrate, as shown in Fig. 3f (*8, 9*). Further exposure to ethylene below 2000 K produced no changes in the LEED pattern, or the Auger spectrum.

The results for the LEED–AES study are summarized in Table 1 and Fig. 3. The W(100)–$\begin{pmatrix} 3 & 0 \\ 1 & -1 \end{pmatrix}$C and the W(100)–$(5 \times 1)$C structures were found to be relatively stable and easily reproduced; hence, they were chosen for the study of the adsorption of H_2 and CO.

3.2. Adsorption and Desorption of Hydrogen

Hydrogen was first adsorbed on clean W(100) at 250 K. In agreement with

[1] The matrix notation suggested by Park and Madden is employed here (*16*).

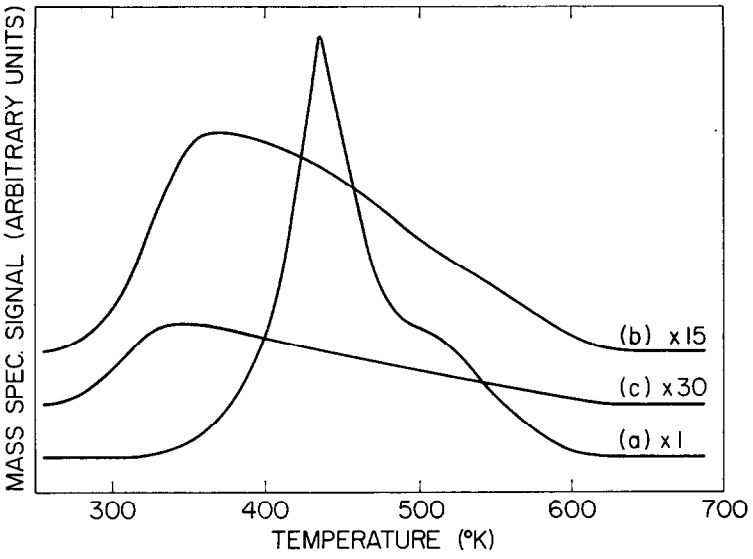

FIG. 4. Hydrogen desorption spectra for: (a) clean W(100), 10 L exposure; (b) W(100)-$\begin{pmatrix} 3 & 0 \\ 1 & -1 \end{pmatrix}$C, 10^4 L exposure; (c) W(100)-(5 × 1)C, 10^4 L exposure.

previous work, two desorption peaks were observed (*19*, *20*). For coverages less than 1.5×10^{14} molecules/cm^2 a second order peak (β_2) was isolated at 535 K. The activation energy for desorption from this state was found from the variation of peak temperature with heating rate to be 32.5 kcal/mole, with a preexponential factor of 0.02 cm^2/mole/sec. At higher exposures of hydrogen the first-order β_1 state at 440 K was populated. The activation energy for desorption from the β_1 state was found from heating rate variation to be 26.5 kcal/mole with a corresponding preexponential factor of 2×10^{13} sec^{-1}. Saturation coverage of hydrogen was measured to be 7.4×10^{14} molecules/cm^2. The relative amount desorbed from the β_1/β_2 states at saturation was 2:1.

The formation of a surface carbide reduced the amount of hydrogen adsorbed dramatically. Desorption spectra for hydrogen from W(100)-$\begin{pmatrix} 3 & 0 \\ 1 & -1 \end{pmatrix}$C and W(100)-(5 × 1)C are shown in Fig. 4. Saturation coverage after exposure to 10^4 L H_2 was 1.5×10^{14} molecules/cm^2 on W(100)-$\begin{pmatrix} 3 & 0 \\ 1 & -1 \end{pmatrix}$C and less than 3.0×10^{13} molecules/cm^2 on W(100)-(5 × 1)C. The very broad peaks prohibited the determination of any kinetic parameters. In order to ascertain the limitation to adsorption of hydrogen, the adsorption of H atoms generated with the hot filament in the mass spectrometer was studied. On clean tungsten no differences in the desorption spectra were found; however, adsorption on the carburized surfaces was enhanced by an order of magnitude over an equivalent 10^4 L exposure without atom generation, indicating an appreciable activation barrier for dissociative hydrogen adsorption on the carbide surface.

3.3. Adsorption and Desorption of Carbon Monoxide

Initially CO adsorbed on clean W(100) in the strongly bound β state, which desorbed between 1000 and 1400 K. After heating to 1500 K the surface was restored to its clean state. Higher exposures to CO filled the β state and resulted in the subsequent appearance of a low temperature CO(α) peak at 377 K, in agreement with others (*13*, *28*). Saturation coverage in the

α state was found to be 7.6×10^{14} molecules/cm^2. The CO(α) desorption peak could not be described by a simple first-order desorption process. Rather, there appeared to be a range of binding energies for the CO(α) state the average of which was estimated to be 22 kcal/mole (92 kJ/mole) by assuming a preexponential factor of 10^{13} s^{-1}.

On the carbide surfaces the amount of CO(β) adsorbed decreased with increasing carburization, while the population of the α state increased, as evidenced by flash desorption and AES. The coverages for the CO(β) state on the clean and two carbide surfaces were calculated from the oxygen signal of the Auger spectra taken after heating to 800 K (see Fig. 5); cov-

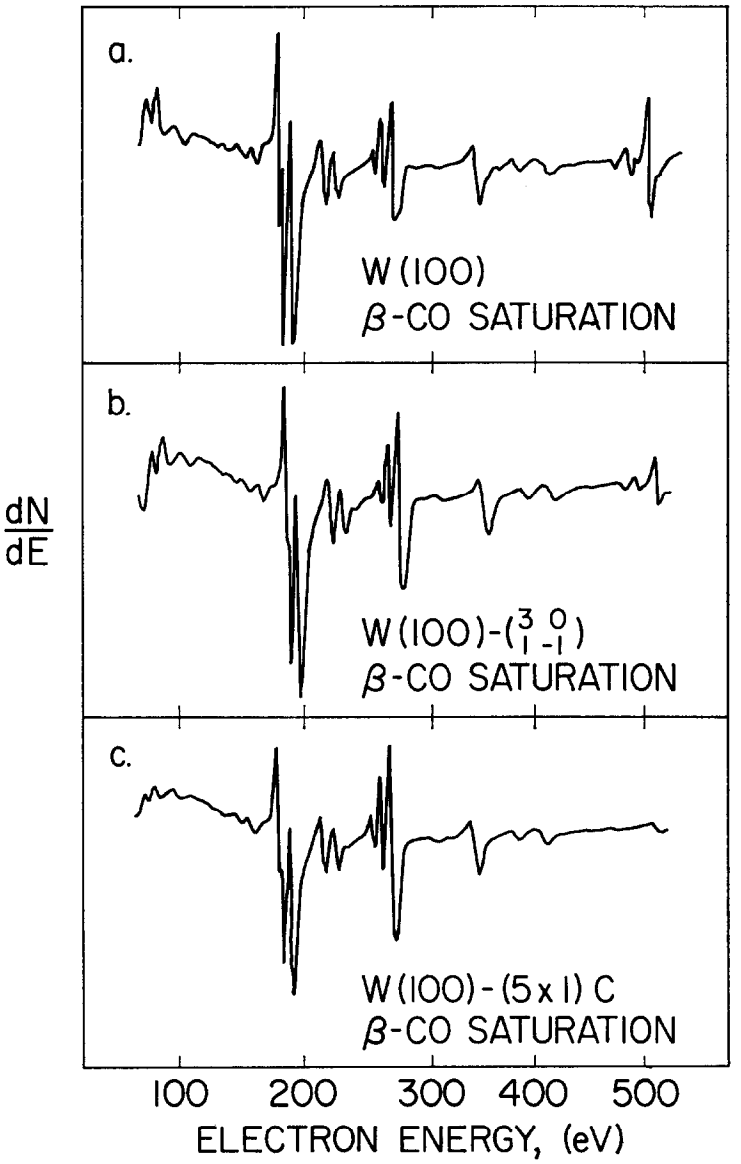

FIG. 5. Auger spectra of CO(β) saturation on: (a) clean W(100); (b) W(100)-$\begin{pmatrix} 3 & 0 \\ 1 & -1 \end{pmatrix}$C; (c) W(100)-(5 × 1)C.

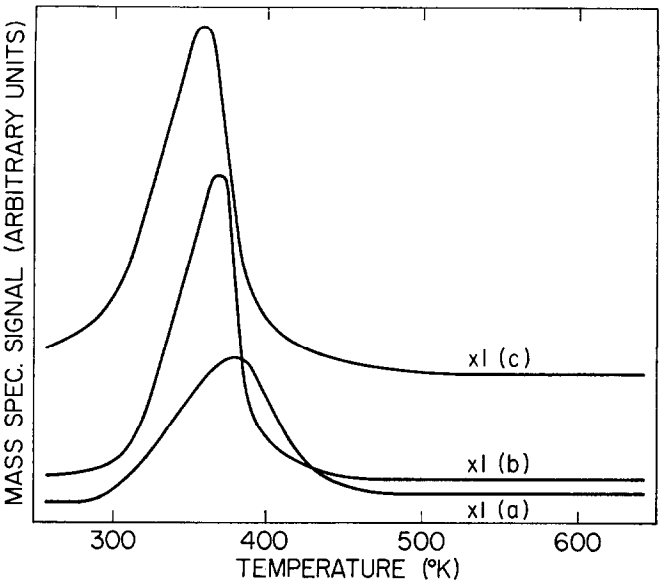

FIG. 6. CO(α) desorption spectra at saturation coverage from: (a) clean W(100), 10 L exposure; (b) W(100)-$\begin{pmatrix} 3 & 0 \\ 1 & -1 \end{pmatrix}$C, 10 L exposure; (c) W(100)-(5 × 1)C, 10 L exposure.

erages in the CO(α) state were determined from flash desorption curves shown in Fig. 6. These results are summarized in Table 2.

Desorption of CO(α) from W(100)-(5 × 1)C appeared to be a simple first-order process. A plot of ln(rate) vs ln(coverage) at constant temperature resulted in a linear plot, the slope of which gave a reaction order of unity. The kinetic parameters were determined from heating rate variation and peak shape analysis; the activation energy for desorption was 19.6 kcal/mole (82 kJ/mole) with a preexponential factor of 5×10^{12} sec^{-1}. The Auger spectra indicated the W(100)-(5 × 1)C surface did not adsorb any CO in the dissociated β state.

The W(100)-$\begin{pmatrix} 3 & 0 \\ 1 & -1 \end{pmatrix}$C surface adsorbed CO into both α and β states. The amount of β-CO adsorbed was less than on the clean surface, and the desorption peaks were at lower temperature. All the CO(β) desorbed by 1300 K on the W(100)-$\begin{pmatrix} 3 & 0 \\ 1 & -1 \end{pmatrix}$C surface. Desorption from the CO(α) state could not be described by a simple first-order reaction. The CO(α) desorption peak on the W(100)-$\begin{pmatrix} 3 & 0 \\ 1 & -1 \end{pmatrix}$C surface displayed characteristics similar to that on the clean surface. The activation energy for desorption was estimated as 21 kcal/mole (88 kJ/mole) by assuming a preexponential factor of 10^{13} sec^{-1}.

4. DISCUSSION

4.1. Carburization of Tungsten

The initial carburization of W(100) paralleled the behavior observed for other body-centered cubic metals. The $c(2 \times 2)$

TABLE 2

Surface	CO(β) saturation/ cm^2	CO(α) saturation/ cm^2
W(100)	4.3×10^{14}	7.6×10^{14}
W(100)-$\begin{pmatrix} 3 & 0 \\ 1 & -1 \end{pmatrix}$C	1.7×10^{14}	9.5×10^{14}
W(100)-(5 × 1)C	0	1.2×10^{15}

structure followed by the $\begin{pmatrix} 3 & 0 \\ 1 & -1 \end{pmatrix}$ structure was observed for Fe(100) (*21*) and Mo(100) (*22*) as well as W(100). Guillot *et al.* (*22*) also observed this structure to occur at $\frac{2}{3}$ monolayer coverage and proposed a structure identical to that shown in Fig. 3c. The proposed configuration for the structure required movement of carbon atoms from their positions in the $c(2 \times 2)$ structure.

The observed splitting of the $(\frac{1}{2}, \frac{1}{2})$ diffraction spots suggested that ethylene dissociated with the carbon atoms filling in the open rows along the (011) direction on the $c(2 \times 2)$ lattice. These additional carbon atoms push the carbon atoms apart in the (010) and (001) directions which resulted in the double row configuration shown in Fig. 3c. Relaxation of the surface structure by a periodic compression and expansion of the rows of tungsten atoms in the $(0\bar{1}1)$ direction may further reduce the repulsive interactions.

Further carburization of the surface only took place at elevated temperatures, indicating a substantial energy barrier for the formation of the ditungsten carbide. Orton (*23*) reports the free energy of formation of W_2C to be $2100 - 2.15T$ cal/mole so that its formation below 1000 K is prohibited by thermodynamics. The apparent stability of the W_2C overlayer observed in these experiments is probably due to a kinetic limitation to decomposition. The identical Auger spectra for W(100)–(5 × 1)C and W(110)–(15 × 3)-R14°C support the contention that a ditungsten carbide overlayer formed on both surfaces. The proposed model of the carbon atoms sitting beneath the surface is similar to that suggested by Estrup and Anderson (*24*) for oxygen adsorption on W(100). They observed that oxygen is adsorbed on top of the tungsten substrate at room temperature. At elevated temperatures they found the oxygen penetrated the surface forming a reconstructed layer. The formation of the W_2C overlayer on W(100) resulted in an increase of the tungsten atom density at the surface to 1.2×10^{15} cm^{-2}. The increased surface atom density caused facet planes to grow, accounting for the observed faceting of the W(100) surface.

4.2. Adsorption and Desorption of Hydrogen

The results reported here for hydrogen desorption from clean W(100) are in excellent agreement with those reported by others (*19*, *20*). The decrease in hydrogen adsorption with increasing carburization has been observed for the nickel carbon (*25*, *26*) system as well as the tungsten carbon system. The hydrogen desorption peaks for both systems broadened out, with no well-defined structure. Since the amount of hydrogen adsorbed could be increased by using H atoms instead of H_2, the limitation to adsorption was ascribed to the dissociation of hydrogen molecules.

4.3. Adsorption and Desorption of Carbon Monoxide

Recently there has been a significant advance in the understanding of CO adsorption on tungsten. ESCA work by Yates *et al.* (*27*) and Menzel (*13*) showed conclusively that the β state of CO is dissociately adsorbed, whereas the α state is molecularly adsorbed. The results presented here are consistent with the suggestion of Froitzheim *et al.* (*28*) that the dissociative adsorption of CO on W(100) required adjacent sites with fourfold symmetry. The density of these site pairs on W(100) is 5×10^{14} cm^{-2}. On clean W(100), CO(β) saturation is less than 5.0×10^{14} molecules/cm^2 due to the random adsorption of CO, isolating single fourfold sites which cannot dissociately adsorb CO. The W(100)–$\begin{pmatrix} 3 & 0 \\ 1 & -1 \end{pmatrix}$C surface has 1.7×10^{14}/cm^2 pairs of adjacent sites available which agrees with the measured CO(β) saturation coverage of 1.7×10^{14} molecules/cm^2 on that surface. The W(100)–(5 × 1)C

surface had no appropriate sites available for CO(β) adsorption and no dissociative adsorption was found.

The presence of carbon or oxygen on W(100) caused the surface to be passivated toward dissociative adsorption of CO. There was a strong correlation between the number of sites passivated by either CO(β) or carbon and the saturation population of the α state as summarized in Table 3. The carburization of W(100) increased the density of sites that were passivated resulting in the increased adsorption of molecular CO. The means by which the surface was passivated, either by carburization or adsorption of CO(β), affected the kinetics for desorption of CO(α). The W(100)–(5 × 1)C surface is homogeneous, so one would expect simple first-order desorption as was found. However, in the case where dissociated CO passivated some of the adsorption sites each of these sites has a slightly different local environment depending on the number and nature of its nearest neighbors. The heterogeneity of the surface resulted in a range of binding energies so the desorption process did not appear to be a simple first-order process.

TABLE 3

Surface	Number passivated sites (cm^{-2})	CO(α) saturation (cm^{-2})
W(100)	8.6×10^{14}	7.6×10^{14}
W(100)-$\begin{pmatrix} 3 & 0 \\ 1 & -1 \end{pmatrix}$C	1.0×10^{15}	9.5×10^{14}
W(100)-(5 × 1)C	1.2×10^{15}	1.2×10^{15}

5. SUMMARY

The initial carburization of W(100) proceeded in a similar fashion to other BCC metals, producing a $c(2 \times 2)$ structure at $\frac{1}{2}$ monolayer and reconstructed to a $\begin{pmatrix} 3 & 0 \\ 1 & -1 \end{pmatrix}$ structure at $\frac{2}{3}$ coverage. This surface structure was inert to further carburization below 1000 K. Heating the crystal to 1500 K in ethylene resulted in the formation of an interstitial carbon structure having the structure of ditungsten carbide at the surface.

The formation of a surface carbide reduced the ability of the surface to dissociate hydrogen, though hydrogen adsorption was enhanced utilizing H atoms. Dissociative adsorption of CO was also inhibited by the surface carbide. Passivation of the surface by carbon enhanced the nondissociative adsorption of CO.

ACKNOWLEDGMENTS

The authors gratefully acknowledge the support of the National Science Foundation through the Center for Materials Research at Stanford (NSF-ENG-76-00726). We also wish to express our appreciation for National Science Foundation Equipment Grant NSF-ENG-75-14191, without which this work could not have been accomplished.

REFERENCES

1. Madix, R. J., *Catal. Rev.—Sci. Engrg.* **15**, 293 (1977).
2. Boudart, M., and Levy, R., *Science* **181**, 547 (1973).
3. Bohm, H., *Electrochim. Acta* **15**, 1273 (1970).
4. Ross, P. N., and Stonehart, P., *J. Electroanal. Chem.* **63**, 450 (1975).
5. Ross, P. N., and Stonehart, P., *J. Catal.* **39**, 298 (1975).
6. Ross, P. N., and Stonehart, P., *J. Catal.* **48**, 42 (1977).
7. Boudart, M., and Imura, K., private communication.
8. Boudart, M., and Ollis, D. F., *Surface Sci.* **23**, 320 (1970).
9. Bauer, E., *Surface Sci.* **7**, 351 (1967).
10. Chen, J., and Papageorgoupoulos, P. A., *Surface Sci.* **20**, 195 (1970).
11. Sharp, L. N., and Scheiber, E. J., *J. Appl. Phys.* **38**, 3320 (1967).
12. Stern, R. M., *Appl. Phys. Lett.* **5**, 218 (1964).
13. Menzel, D., presented at the Third ISISS Conference (1977).
14. Housley, M., and King, D. A., *Surface Sci.* **62**, 81 (1977).
15. Clavenna, L. R., and Schmidt, L. D., *Surface Sci* **33**, 11 (1972).
16. Park, R. L., and Madden, H. H., *Surface Sci.* **11**, 188 (1968).

17. Wycoff, R. W. G., "Crystal Structures," Vol. 1. Wiley–Interscience, New York, 1964.
18. Ertl, G., and Kuppers, J., "Low Energy Electron and Surface Chemistry." Springer–Verlag, New York, 1974.
19. Tamm, P., and Schmidt, L. D., *J. Chem. Phys.* **51**, 5352 (1969).
20. Madey, T. E., and Yates, J. T., Colloque International sur la Structure et les Properties des Surfaces des Solids CNRS (1969).
21. Benziger, J. B., and Madix, R. J., to appear.
22. Guillot, C., Riwan, R., and Lecante, J., *Surface Sci.* **59**, 581 (1976).
23. Orton, G. W., *Trans. Metallurgical Soc. AIME* **230**, 600 (1964).
24. Estrup, P. J., and Anderson, J., "Report on the Proceedings of the 27th Annual Physical Electronics Conference," p. 67. MIT Press, Cambridge, Mass., 1967.
25. McCarty, J. G., and Madix, R. J., *Surface Sci.* **54**, 121 (1976).
26. Ko, E., and Madix, R. J., to appear.
27. Yates, J. T., Madey, T. E., and Erickson, N. E., *Surface Sci.* **43**, 257 (1974).
28. Froitzheim, H., Ibach, H., and Lehwald, S., *Surface Sci.* **63**, 56 (1977).